THE JOURNAL OF PHYSICAL CHEMISTRY C

Article

pubs.acs.org/JPCC

Synthesis and Spectroscopic Properties of Monoclinic α-$Eu_2(MoO_4)_3$

V. V. Atuchin,*[,†,‡,§] A. S. Aleksandrovsky,[∥] O. D. Chimitova,[⊥] T. A. Gavrilova,[#] A. S. Krylov,[▽] M. S. Molokeev,[○] A. S. Oreshonkov,[▽] B. G. Bazarov,[⊥] and J. G. Bazarova[⊥]

[†]Laboratory of Optical Materials and Structures, Institute of Semiconductor Physics, SB RAS, Novosibirsk 630090, Russia

[‡]Functional Electronics Laboratory, Tomsk State University, Tomsk 634050, Russia

[§]Laboratory of Semiconductor and Dielectric Materials, Novosibirsk State University, Novosibirsk 630090, Russia

[∥]Laboratory of Coherent Optics, Kirensky Institute of Physics, SB RAS, Akademgorodok, Krasnoyarsk 660036, Russia

[⊥]Laboratory of Oxide Systems, Baikal Institute of Nature Management, SB RAS, Ulan-Ude 670047, Russia

[#]Laboratory of Nanodiagnostics and Nanolithography, Institute of Semiconductor Physics, SB RAS, Novosibirsk 630090, Russia

[▽]Laboratory of Molecular Spectroscopy, Kirensky Institute of Physics, SB RAS, Krasnoyarsk 660036, Russia

[○]Laboratory of Crystal Physics, Kirensky Institute of Physics, SB RAS, Krasnoyarsk 660036, Russia

Supporting Information

ABSTRACT: The microcrystals of monoclinic europium molybdate, α-$Eu_2(MoO_4)_3$, have been fabricated by solid-state synthesis at T = 753−1273 K for 300 h. The crystal structure of α-$Eu_2(MoO_4)_3$ has been refined by the Rietveld method and was found to belong to the space group $C2/c$ with unit cell parameters a = 7.5576(1), b = 11.4709(2), c = 11.5158(2) Å, and β = 109.278(1)° (R_B = 3.39%). About 40 narrow Raman lines have been observed in the Raman spectrum of the α-$Eu_2(MoO_4)_3$ powder sample. The luminescence spectra of α-$Eu_2(MoO_4)_3$ under excitation at 355 and 457.9 nm reveal domination of induced electric dipole transition $^5D_0 \rightarrow {}^7F_2$ and the presence of ultranarrow lines at $^5D_0 \rightarrow {}^7F_0$ and $^5D_1 \rightarrow {}^7F_0$ transitions.

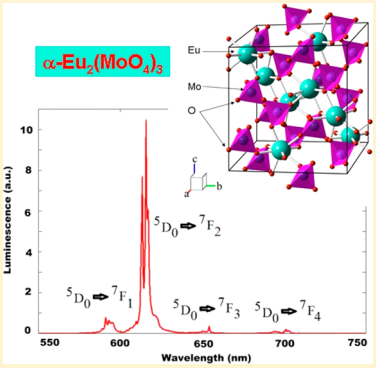

1. INTRODUCTION

Molybdate crystals are presently the subject of considerable interest and detailed evaluation because of their valuable structural, thermal, electrical, and spectroscopic properties which are promising for practical applications in advanced electronic and photonic technologies.[1−8] The rare-earth molybdate crystals or those doped with rare-earth ions are of special interest because of their specific spectroscopic properties and potential application as laser and luminescent hosts.[6,8−16] As a rule, the rare-earth ions in molybdates are in low-symmetry positions, and this is a key factor for the creation of efficient luminescent media. The crystals containing trivalent europium ions are of particular interest because these ions produce efficient red photoluminescence necessary for the creation of white-light emitting diodes (WLED) devices with the spectral characteristics similar to sun daylight.[17−24] In the present photonics, many different Eu^{3+}-doped compounds with complex structures are evaluated as phosphors, but the Eu^{3+} doping level used is typically low. In many cases, the crystallographic positions of Eu^{3+} ions may not be evident, and it is difficult to see clearly the relation between the photoluminescence spectrum and crystallographic environment of the Eu^{3+} ions. The compounds with stoichiometric europium content are more suitable for this purpose because the Eu^{3+} ion position can be reliably defined from crystal structure analysis. The scheelite-type modification of europium molybdate, α-$Eu_2(MoO_4)_3$, is among the compounds where Eu^{3+} ions are in a low symmetry position.[25]

Europium molybdate belongs to a wide family of $Ln_2(MoO_4)_3$ compounds whose intriguing physical properties have been under investigation for many years.[26] Generally, the molybdates possess a sequence of phase transitions with temperature variation, and the β and β' modifications are noncentrosymmetric.[26−29] Low-temperature monoclinic α-$Eu_2(MoO_4)_3$, belonging to space group $C2/c$, appears at temperatures below ∼470 K.[25,30] The crystal structure of α-$Eu_2(MoO_4)_3$ is shown in Figure 1.[25,31] The structure can be considered as a framework formed by MoO_4 tetrahedrons and EuO_8 polyhedrons linked by corners. The unit cell is large, including 68 atoms, and possesses cell volume as high as V = 941.60 $Å^3$.[25] This monoclinic modification of $Eu_2(MoO_4)_3$ is isostructural to $Eu_2(WO_4)_3$, and these compounds are able to form a continuous series of the solid solutions with $Eu_2(Mo_{1-x}W_x)_3O_{12}$ composition.[32,33]

Received: April 26, 2014
Revised: June 9, 2014
Published: June 10, 2014

Downloaded via STATE PUBLIC SCI TECHN LIB on October 29, 2020 at 10:38:24 (UTC).
See https://pubs.acs.org/sharingguidelines for options on how to legitimately share published articles.

© 2014 American Chemical Society

dx.doi.org/10.1021/jp5040739 | J. Phys. Chem. C 2014, 118, 15404−15411

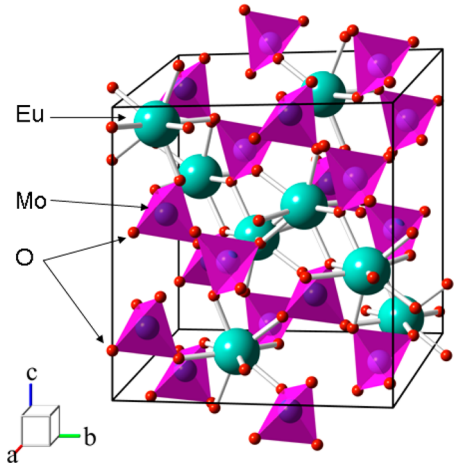

Figure 1. Crystal structure of α-$Eu_2(MoO_4)_3$. Unit cell is outlined. Lone atoms are omitted for clarity.

The thermal and structural properties of low-temperature modification α-$Eu_2(MoO_4)_3$ were reported in several studies.[25,30,34] Generally, there are several modifications found for $Eu_2(MoO_4)_3$. Monoclinic phase α-$Eu_2(MoO_4)_3$ is stable at low temperatures, and upon heating this modification undergoes the transition to tetragonal modification β-$Eu_2(MoO_4)_3$ (space group $P\bar{4}2_1m$) at ∼1180 K.[30] However, the $\beta \rightarrow \alpha$ transition is frustrated upon cooling because of low mobility of metallic cations. Above this, the formation of metastable β'-$Eu_2(MoO_4)_3$ belonging to the space group *Pba*2 was detected at ∼470 K.[30] β'-$Eu_2(MoO_4)_3$ is so stable that even single crystals have been grown and evaluated.[34−37] This indicates that the preparation of a pure phase of α-$Eu_2(MoO_4)_3$ modification is not a trivial technological task. Physical properties of this modification are practically unknown, except for structural parameters and magnetic susceptibility.[25,38] It is known from available structural data that in the α-$Eu_2(MoO_4)_3$ lattice the europium atoms are in a single inequivalent position with symmetry C_1. This is the limiting case of the Eu^{3+} lowest-symmetry environment in crystals, and vibrational and photoluminescent parameters of such emission centers are of particular interest. Therefore, the aim of the present study is the synthesis and detailed evaluation of structural and spectroscopic properties of α-$Eu_2(MoO_4)_3$ molybdate.

2. EXPERIMENTAL METHODS AND DATA PROCESSING

Depending on the preparation route, europium trimolybdate can be obtained in either low-temperature α-form or high-temperature β-form. In particular, the low-temperature europium molybdate was chemically synthesized by a two-step procedure. The powder α-$Eu_2(MoO_4)_3$ sample was prepared from stoichiometric amounts of MoO_3 (99.99%, Red Chemist, Ltd., Russia) and Eu_2O_3 (99.99%, Red Chemist, Ltd., Russia). First of all, before being weighed, Eu_2O_3 and MoO_3 were annealed at T = 1273 K and T = 923 K, respectively, for 12 h to remove excessive moisture and carbon dioxide impurities. Then, the preheated powders were weighted in stoichiometric amounts. After this, the starting oxides were thoroughly mixed with ethyl alcohol in an agate mortar and reacted at the temperatures of 753 and 823 K for 30 and 200 h, respectively. After cooling to the room temperature, the samples were ground in an agate mortar and heated to 923 and 1273 K for 50 and 20 h, correspondingly, yielding a light cream-colored α-$Eu_2(MoO_4)_3$. Phase purity of the intermediate and final products was confirmed by X-ray diffraction (XRD) measurements using Cu K_α radiation. Micromorphology of the final product was observed by scanning electron microscopy (SEM) with the help of a LEO 1430 electron microscope.

The thermal behavior of europium molybdate was examined by differential scanning calorimetry (DSC) using a Netzsch STA 449 F1 Jupiter device in the temperature range of 293−1423 K. The compound was placed into a Pt crucible and heated and cooled in Ar atmosphere at 10 K/min. To test the reproducibility, the heating−cooling cycles were repeated twice. Each heating process was started at 293 K and finished at 1423 K.

The X-ray powder diffraction of $Eu_2(MoO_4)_3$ was measured at room temperature on a D8 ADVANCE Bruker diffractometer (VANTEC linear detector, Cu K_α radiation). Because the $Eu_2(MoO_4)_3$ powder pattern was measured at room temperature, the cell parameters and atom coordinates of the monoclinic phase were used as a starting model for the structure refinement.[25] The TOPAS 4.2 program was used for the Rietveld refinement.[39]

The unpolarized Raman spectra were collected in a backscattering geometry using triple-monochromator Horiba Jobin Yvon T64000 triple Raman spectrometer operating in double-subtractive mode using a liquid-nitrogen-cooled charge-coupled detector. The spectral resolution for Stokes side Raman spectra was set to ∼4 cm^{-1} (this resolution was achieved using gratings with 1800 grooves/mm and 100 μm slits). The microscope system based on the Olympus BX41 microscope with an Olympus 50× objective lens with focal length f = 0.8 mm and NA = 0.75 numerical aperture provided a focal spot diameter on the sample of approximately 2 μm.[40,41] The 457.9 nm line from a Spectra-Physics Stabilite 2017 single-mode Ar^+ laser was used as a light excitation source; the power level on the sample was 5 mW. This level of laser light intensity was adjusted to avoid sample heating. The positions and widths of spectral lines were obtained by least-squares fitting of the experimental data to the Lorentzian equation[42]

$$I_L = \frac{A}{1 + \left(\frac{x-\omega}{\Gamma}\right)^2}$$

where I_L is intensity, A is amplitude, ω is wavenumber, Γ is full width at half-height, and x is actual coordinate (wavenumber).

Luminescence spectra were taken using either a LOMO DFS-24 double spectrometer providing spectral resolution of 3 cm^{-1}, with excitation by a LaserCompact LCS-DTL-374QT DPSS laser generating 20 mW power at 355 nm, or a Horiba Jobin-Yvon T64000 triple Raman spectrometer with argon laser excitation at 457.9 nm with power 3 mW at sample. In the the latter case, the spectral resolution was either 2.7 or 0.4 cm^{-1}, depending on the measurement requirements.

3. RESULTS AND DISCUSSION

The final powder product prepared by the synthesis route described above is of a light-cream color typical of europium oxides.[43,44] The particle micromorphology of the product is shown in Figure 2. The formation of well-faceted grains with the size 1−5 μm is evident. This characteristic size and crystal habit was predestined by the synthesis conditions selection. When the temperature is close to the range of effective evaporation of molybdenum oxide in the air and the synthesis

dx.doi.org/10.1021/jp5040739 | J. Phys. Chem. C 2014, 118, 15404−15411

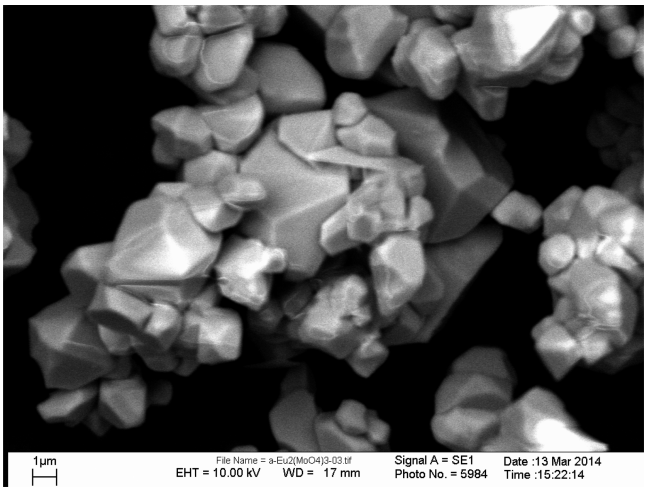

Figure 2. SEM pattern of α-$Eu_2(MoO_4)_3$ microcrystals.

time is long enough, the equilibrium molybdate crystal forms with developed facets appear because of activated diffusion and possible local vapor-phase mass transport.[15,45−47] As a rule, for volatile compounds, well-faceted habit formation during annealing is a reliable indicator of high structural quality at micro- and nanocrystalline scale.[48−52]

The phase purity of the α-$Eu_2(MoO_4)_3$ powder sample was verified by XRD measurements and structure refinement. The recorded XRD pattern is shown in Figure 3. The refinement

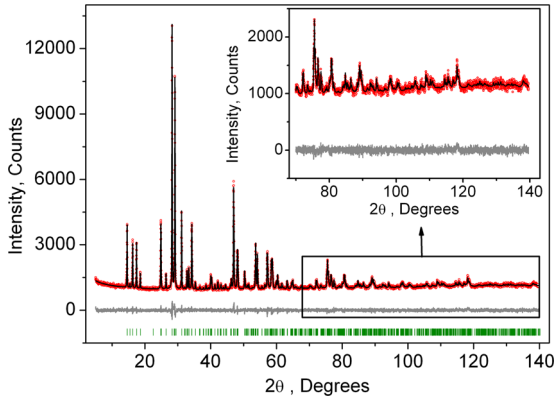

Figure 3. Rietveld difference plot of α-$Eu_2(MoO_4)_3$ at room temperature.

was stable and gives low *R*-factors (Table 1). All atoms were refined with isotropic thermal parameters. All oxygen atoms were refined to have the same thermal parameter. The atom coordinates and thermal parameters are shown in Table 2. All bond lengths obtained by the refinement are depicted in Table 3. The values are in good relation to those earlier reported for the α-$Eu_2(MoO_4)_3$ phase.[25]

The DSC curve recorded from $Eu_2(MoO_4)_3$ is shown in Figure 4. Two endothermic signals at 1182 and 1398 K were detected upon sample heating. During cooling, $Eu_2(MoO_4)_3$ shows an exothermic effect confirming the crystallization temperature at 1373 K. The difference between melting and crystallization temperatures seems to appear because of the supercooling effect. It should be pointed out that the melting temperature measured in the present experiment is noticeably lower than that earlier reported, falling in the range of 1417−

Table 1. Main Parameters of Processing and Refinement

space group	*C*2/*c*
a (Å)	7.5576(1)
b (Å)	11.4709(2)
c (Å)	11.5158(2)
β (deg)	109.278(1)
V (Å^3)	942.36(3)
2θ interval (deg)	5−140
number of reflections	901
number of refined parameters	67
R_{wp} (%)	3.39
R_p (%)	2.67
R_B (%)	0.84
χ^2	1.17

Table 2. Atom Coordinates and Isotropic Thermal Parameters (B_{iso}) of the α-$Eu_2(MoO_4)_3$ Structure

	x	*y*	*z*	B_{iso}
Eu	0.3334 (7)	0.3758 (3)	0.4091 (2)	1.65 (10)
Mo1	0	0.1259 (6)	0.25	0.70 (14)
Mo2	0.1484 (7)	0.3877 (3)	0.0594 (2)	1.25 (12)
O1	0.160 (3)	0.0419 (13)	0.217 (2)	1.4 (2)
O2	0.139 (4)	0.2112 (16)	0.3926 (16)	1.4 (2)
O3	0.254 (3)	0.3196 (13)	0.1964 (14)	1.4 (2)
O4	0.362 (3)	0.4544 (14)	0.045 (2)	1.4 (2)
O5	0.046 (4)	0.4659 (16)	0.3979 (15)	1.4 (2)
O6	0.459 (3)	0.2123 (14)	0.062 (2)	1.4 (2)

Table 3. Main Interatomic Distances (Å) in the α-$Eu_2(MoO_4)_3$ Structure at Room Temperature[a]

Eu−O1^{i}	2.404 (18)	Eu−O6^{iii}	2.398 (16)
Eu−O2	2.36 (2)	Mo1−O1	1.685 (17) × 2
Eu−O2^{ii}	2.436 (18)	Mo1−O2	1.902 (18) × 2
Eu−O3	2.410 (15)	Mo2−O3	1.704 (15)
Eu−O4^{iii}	2.367 (18)	Mo2−O4	1.842 (18)
Eu−O4^{iv}	2.460 (19)	Mo2−O5^{v}	1.92 (2)
Eu−O5	2.37 (2)	Mo2−O6^{vi}	1.78 (2)

[a]Symmetry elements: (i) $-x + 1/2, y + 1/2, -z + 1/2$; (ii) $-x + 1/2, -y + 1/2, -z + 1$; (iii) $-x + 1, y, -z + 1/2$; (iv) $x, -y + 1, z + 1/2$; (v) $-x, y, -z + 1/2$; (vi) $-x + 1/2, -y + 1/2$.

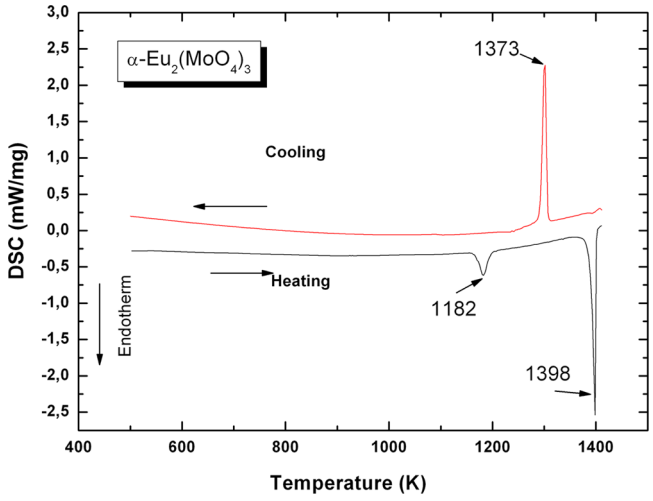

Figure 4. DSC results obtained from α-$Eu_2(MoO_4)_3$.

dx.doi.org/10.1021/jp5040739 | J. Phys. Chem. C 2014, 118, 15404−15411

1444 K.[26,30,34] The expected exothermic peak at ~1182 K was not found during sample cooling. Nevertheless, during the next heating with the rate of 5 K/min, the endothermic peak was reproduced at 1183.4 K. The existence of two phase transitions at 434−453 K[1,30,34] and 1130−1173 K[1,3,25,26,30,34] was mentioned in the literature. The transition at 1183 K observed in the present experiment is in reasonable agreement with higher-temperature transition range of 1130−1173 K. Alternatively, any signature that may be attributed to the lower-temperature transition range of 434−453 K was not detected. According to the XRD analysis, after DSC measurement and cooling, the sample transforms from α- to β'-$Eu_2(MoO_4)_3$ crystal structure with space group *Pba*2. The structural parameters of β'-$Eu_2(MoO_4)_3$ were supposed to be analogous to those of the known phase β'-$Gd_2(MoO_4)_3$ belonging to the same space group *Pba*2.[53] Thus, the selected cooling rate of 10 K/min results in the high-temperature phase quenching.

The Raman spectrum obtained from α-$Eu_2(MoO_4)_3$ powder is shown in Figure 5. About 40 narrow Raman lines were

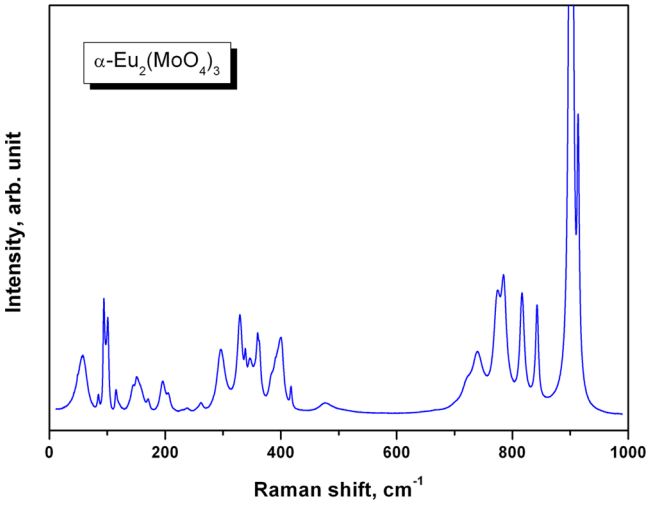

Figure 5. Raman spectrum of α-$Eu_2(MoO_4)_3$.

revealed by the experimental spectrum fitting, and the total set of Raman lines found in α-$Eu_2(MoO_4)_3$ is shown in Table 4. The Raman spectrum of α-$Eu_2(MoO_4)_3$ can be divided into two parts with a wide empty gap in the range 500−700 cm^{-1} that is commonly observed in molybdates with MoO_4 tetrahedrons.[4,9,10,14,16,28,46,54] More detailed spectra within low- and high-wavenumber ranges are shown in Figures 1S and 2S of Supporting Information together with the results of component decomposition. In the range of stretching vibrations of MoO_n polyhedra (720−940 cm^{-1}), where n = 4 or 6, many lines were observed because of the presence of several independent (and perhaps inequivalent) and distorted MoO_4 tetrahedrons. The most intense line is detected at 901.4 cm^{-1}. It should be pointed out that, up to now, only low-resolution Raman spectra have been recorded under excitation at 514.5 nm.[37] The use of the excitation at 514.5 nm is not suitable for Eu-bearing compounds because the appearance of photoluminescence lines is possible over the range of 534−542 nm and there is overlap with Raman lines. This effect is shown in Figure 3S and 4S of Supporting Information via comparison of spectra obtained with excitation at 514.5 and 457.8 nm.

Vibrational representation for the monoclinic phase at the center of the Brillouin zone is

$$\Gamma_{vibr} = 25A_g + 25A_u + 26B_g + 26B_u \quad (1)$$

Acoustic and optic modes are

$$\Gamma_{acoustic} = A_u + 2B_u \quad (2)$$

$$\Gamma_{optic} = 25A_g + 24A_u + 26B_g + 24B_u \quad (3)$$

Infrared and Raman active modes are

$$\Gamma_{raman} = 25A_g + 26B_g \quad (4)$$

$$\Gamma_{infrared} = 25A_u + 26B_u \quad (5)$$

To calculate the α-$Eu_2(MoO_4)_3$ vibrational spectrum, the program package LADY was used.[55] The atomic vibration values were obtained using the simplified version of the Born−Karman model.[56] Within this model, only the pairwise interactions and bond-stretching force constants $A = (\partial^2 E)/(\partial R^2)$ (E, energy; R, bond length) are considered. A simplified version of the Born−Karman model implies that A depends on R and the $A(R)$ dependencies are the same for all atom pairs:

$$A = \lambda \exp(-r_{ij}/\rho)$$

where r_{ij} is the interatomic distance and λ and ρ are the parameters characterizing the selected pair interaction. To find the model parameters, a special optimization program was written and tested for several compounds.[57−59] The crystal lattice stability conditions were taken into account. The parameters obtained for α-$Eu_2(MoO_4)_3$ are shown in Table 5.

The calculations show that 39 Raman active modes in the range below 500 cm^{-1} and 12 Raman active modes in the range above 700 cm^{-1} should appear. This is in agreement with the selection rules, and calculated parameters of 51 possible Raman active modes are shown in Table 4 in comparison with experimental results. The strong high-wavenumber band at 901.4 cm^{-1} is assigned to the Mo1−O1 symmetric stretching vibration, as illustrated in Figure 6a. The calculations show that the Raman band at 913.8 cm^{-1} should contain three modes: namely, the line at 914 cm^{-1} corresponding to the Mo2−O3 stretching vibration shown in Figure 6b and two small intensity lines at 915.9 and 916.3 cm^{-1} relating to the Mo1−O1 antisymmetric stretching vibrations shown in Figure 6c,d. The Raman band at 842.5 cm^{-1} is a superposition of two lines whose calculated wavenumber values are 843.0 (A_g) and 839.0 (B_g) cm^{-1}. The calculated intensity of B_g mode is much smaller than that of A_g mode, and, probably for this reason, the decomposition of experimental spectra reveals only one line for this band. Both vibrations are assigned to Mo2−O6 stretching. A similar situation is found for the band recorded at 816.8 cm^{-1}, which is expected to be the superposition of two calculated modes 815.5 cm^{-1} (A_g) and 815.5 cm^{-1} (B_g). The calculated intensity of the A_g mode is well above that of the B_g mode. These vibrations correspond to the Mo2−O4 stretching vibration. The band at 773.6 cm^{-1} is assigned to the Mo1−O2 symmetric stretching vibration. The band at 785.1 cm^{-1} corresponds to Mo1−O2 antisymmetric stretching, and the bands at 739.7 and 720.9 cm^{-1} are assigned to Mo2−O5 vibrations.

Taking into account the fact that the atoms are in general positions and the Mo−O lengths are different, normal vibration modes are distorted. The distorted bending modes of MoO_4 originating from undistorted ν_2 and ν_4 modes of MoO_4 are observed within the 230−480 cm^{-1} range. Our calculations indicate the presence of 22 Raman active vibrations within this

dx.doi.org/10.1021/jp5040739 | J. Phys. Chem. C 2014, 118, 15404−15411

Table 4. Calculated and Experimental Relative Magnitudes (I), Wavenumbers, and Full Widths at Half-Maximum (FWHM) for Raman Lines

Number	Symmetry type	I (calc.)	ω, cm^{-1} (calc.)	I (exp.)	ω, cm^{-1} (exp.)	Γ (FWHM), cm^{-1}
1	B_g	5.8	916.3			
2	B_g	5.8	915.9	16.2	913.8	4.2
3	A_g	79.8	914.1			
4	A_g	100.0	901.0	100.0	901.4	5.9
5	A_g	53.5	843.0	7.0	842.5	6.3
6	B_g	1.3	839.0			
7	A_g	22.3	815.5	7.8	816.8	9.3
8	B_g	1.7	815.5			
9	B_g	0.9	794.5	7.6	785.1	12.1
10	A_g	14.7	772.9	6.5	773.6	13.6
11	A_g	43.4	730.0	3.6	739.7	23.3
12	B_g	0.6	728.8	1.2	720.9	18.6
13	A_g	3.5	478.9	0.6	478.7	25.5
14	B_g	0.1	469.0			
15	A_g	0.9	422.5	0.1	418.8	2.2
16	B_g	1.2	421.6			
17	A_g	0.1	398.3	4.4	400.5	9.2
18	B_g	0.2	396.5	2.8	392.1	11.5
19	A_g	11.6	367.8	1.3	383.4	8.3
20	B_g	0.6	358.4	1.9	363.4	4.7
21	B_g	0.3	340.6	3.9	359.7	8.0
22	A_g	14.5	340.0	2.7	347.3	13.4
23	A_g	6.9	331.3	1.8	338.7	3.4
24	B_g	0.3	320.9	6.3	329.1	10.5
25	A_g	5.2	304.9			
26	B_g	0.2	299.7			
27	A_g	4.6	295.9	4.3	296.9	15.5
28	B_g	0.3	283.8			
29	A_g	3.8	278.7			
30	B_g	0.3	265.7	0.4	261.3	5.3
31	B_g	0.6	248.1			
32	A_g	1.2	245.6			
33	B_g	0.6	228.4	0.1	237.7	4.2
34	A_g	2.0	228.2			
35	B_g	0.8	205.5	0.9	205.4	6.9
36	A_g	1.2	202.0	2.1	195.9	8.8
37	B_g	0.3	165.4	0.6	170.7	4.4
38	A_g	0.8	155.8	1.2	158.0	11.3
39	B_g	0.3	152.6	1.7	151.3	8.5
40	A_g	0.3	150.7			
41	A_g	0.8	146.6	1.2	144.0	8.0
42	B_g	0.3	141.9	0.4	119.1	5.0
43	B_g	0.2	123.0	1.3	115.4	2.8
44	B_g	0.1	115.6	5.7	101.2	3.1
45	A_g	0.6	111.6	3.0	98.2	3.7
46	B_g	0.1	98.5	3.6	95.2	2.6
47	A_g	0.1	93.6	5.6	93.8	2.0
48	B_g	0.1	88.7	0.6	85.0	1.4
49	A_g	0.2	88.6	0.4	84.0	1.3
50	A_g	0.1	86.1	2.5	59.2	12.3
51	B_g	0.1	84.9	2.2	52.6	19.2

Table 5. Parameters of the Interatomic Interaction Potential

interaction	λ (aJ/Å^2)	ρ (Å)
Eu−O	317.83	0.3926
Mo1−O1	376.67	0.4038
Mo1−O2	402.67	0.4059
Mo2−O3	408.17	0.4023
Mo2−O4	385.17	0.4056
Mo2−O5	407.67	0.4050
Mo2−O6	395.17	0.4065
O−O	307.67	0.3916

wavenumber range. For example, the experimental line at 383.4 cm^{-1} must be assigned to the distorted ν_2 normal vibration of Mo1 tetrahedron, as shown in Figure 6e. Generally, the frequency of ν_4 vibration should be above that of the ν_2 vibration, and our calculation results are in agreement with this relation.[60] For example, Raman band at 478.7 cm^{-1} consists of two lines that must originate from distorted ν_4 bending mode of MoO_4.

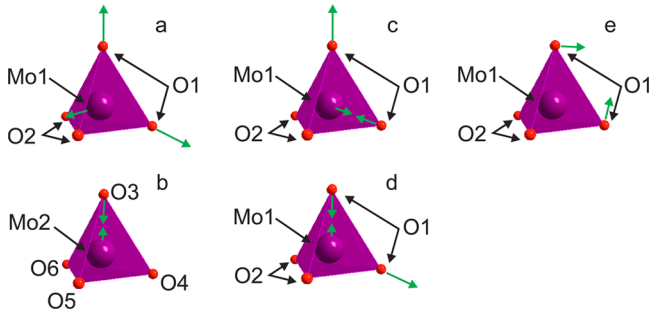

Figure 6. Calculated vibration modes of the MoO_4 tetrahedrons in α-$Eu_2(MoO_4)_3$. (a) A_g 901.0 cm^{-1}, (b) A_g 914.1 cm^{-1}, (c) B_g 916.3 cm^{-1}, (d) B_g 915.9 cm^{-1}, and (e) A_g 367.8 cm^{-1}.

As to the low-wavenumber range of 50−210 cm^{-1}, 17 modes are expected in α-$Eu_2(MoO_4)_3$. This region contains translational, rotational, and mixed vibrations of individual structural units. The bands at 52.6 and 59.2 cm^{-1} are assigned to the Eu translation vibrations.

dx.doi.org/10.1021/jp5040739 | J. Phys. Chem. C 2014, 118, 15404−15411

The most intense part of the photoluminescence spectrum of powder α-$Eu_2(MoO_4)_3$ excited at 355 nm is presented in Figure 7. It contains the Eu^{3+} transitions from the $^5D_0$ level to the ^7F_J

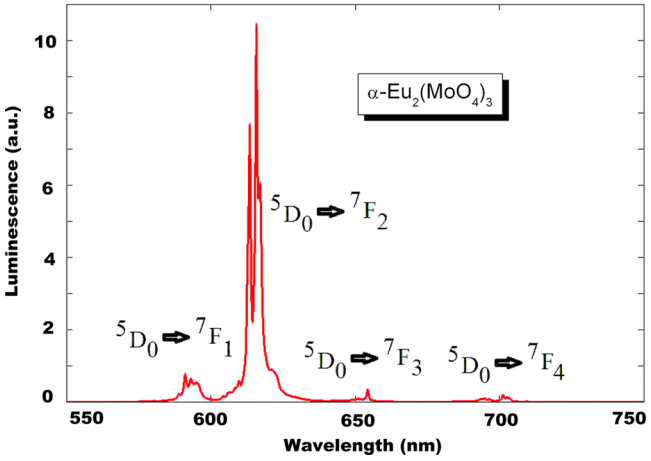

Figure 7. Photoluminescence spectrum from the $Eu^{3+5}D_0$ level in the powder sample of α-$Eu_2(MoO_4)_3$. Excitation wavelength, 355 nm.

manifold. The shape of spectral bands and intensity distribution between different channels is very close to those presented in ref 62 for mesoporous α-$Gd_2(MoO_4)_3$:Eu^{3+}, as well as to those observed in the low-resolution spectrum for nanophosphor of the same chemical formula.[63] The weaker part of Eu^{3+} luminescence excited at 457.9 nm is presented in Figure 8.

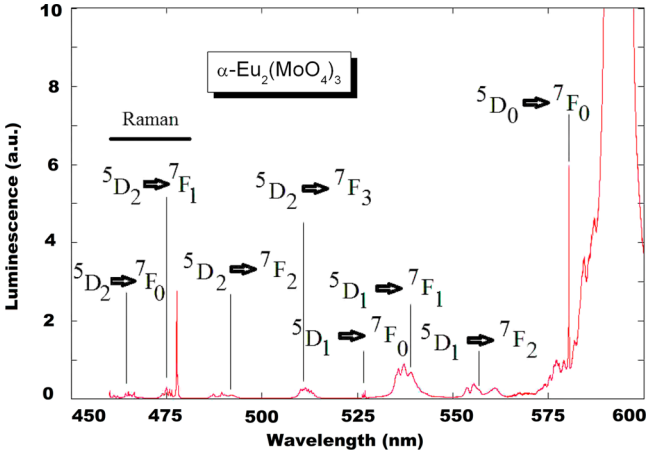

Figure 8. Eu^{3+} luminescence in a α-$Eu_2(MoO_4)_3$ powder sample in the region below 600 nm. Excitation wavelength 457.9 nm. The region below 480 nm is perfectly explained by Raman scattering contribution.

Possible positions of $^5D_2 \rightarrow {}^7F_0$ and $^5D_2 \rightarrow {}^7F_0$ transitions are indicated in Figure 8; however, they were not identified in the present spectrum because the signal observed in the region below 480 nm is perfectly explained by Raman scattering contribution, as can be seen in Figure 3S of Supporting Information. The outstanding feature of the part of spectrum presented in Figure 8 is the ultranarrow line easily identified with the transition between two Stark singlets $^5D_0$ and $^7F_0$. This spectral feature is shown in Figure 9. The line is positioned at 580.38 nm, giving the energy of the $^5D_0$ level at 17 230 cm^{-1} from the ground state. It is 31 cm^{-1} higher than the position of the $Eu^{3+5}D_0$ level in β'-$Gd_{1.99}Eu_{0.01}(MoO_4)_3$.[64] The width of the observed $^5D_0 \rightarrow {}^7F_0$ luminescent line measured at 0.37 cm^{-1}

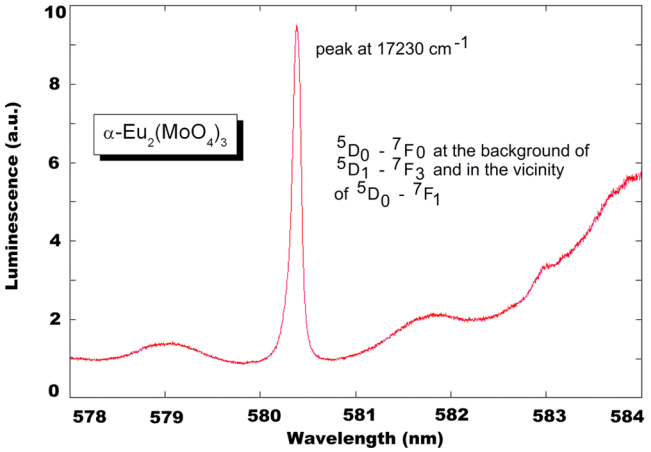

Figure 9. Ultranarrow luminescent line $^5D_0$–$^7F_0$ at the background of $^5D_1$–$^7F_3$ and in the vicinity of the $^5D_0$–$^7F_1$ band.

resolution is equal to 3.3 cm^{-1}. Another set of trident-like ultranarrow lines shown in Figure 10 is found at 526.22, 526.63,

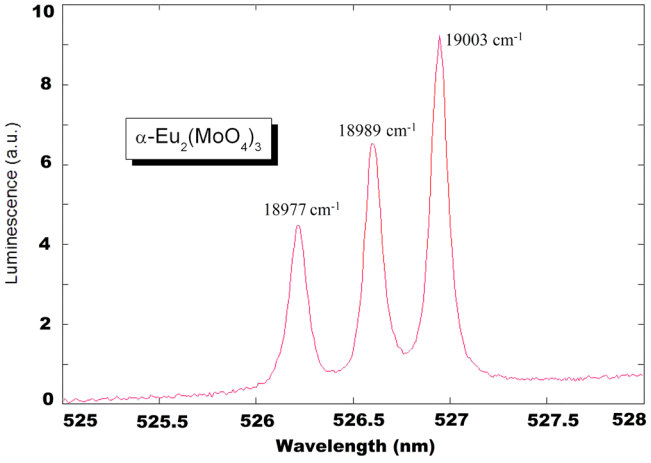

Figure 10. A triplet of ultranarrow luminescent lines $^5D_1$–$^7F_0$ in the vicinity of band $^5D_1$–$^7F_1$.

and 526.96 nm, and this specific set must be assigned to transitions from the Stark triplet $^5D_1$ to $^7F_0$ ground state. The positions of crystal field split $^5D_1$ sublevels in α-$Eu_2(MoO_4)_3$ are, therefore, 18 977, 18 989, and 19 003 cm^{-1}, being several tens of reciprocal centimeters higher than those for one of inequivalent Eu positions in β'-$Gd_{1.99}Eu_{0.01}(MoO_4)_3$.[64] The widths of all three luminescent lines at transition $^5D_1 \rightarrow {}^7F_0$ are on the order of 3 cm^{-1}, too. The observed luminescent features, with the accuracy limited by spectral width of ultranarrow lines, are consistent with a single inequivalent position of Eu^{3+} in the crystal lattice with the local symmetry as low as C_1.

4. CONCLUSIONS

The structural quality of polycrystalline α-$Eu_2(MoO_4)_3$ provides detailed observation of spectroscopic parameters of this molybdate. In the α-$Eu_2(MoO_4)_3$ lattice, Eu^{3+} ions are in the low local symmetry C_1 position. Many narrow lines are found in the Raman spectrum. The distribution of intensities of different luminescent channels in the room-temperature spectrum of α-$Eu_2(MoO_4)_3$ is rather typical of the Eu^{3+}-containing compounds, with the domination of the $^5D_0 \rightarrow {}^7F_2$ channel. Ultranarrow luminescent lines (FWHM ~3 cm^{-1}) are

dx.doi.org/10.1021/jp5040739 | J. Phys. Chem. C 2014, 118, 15404–15411

found at transitions $^5D_0 \rightarrow {}^7F_0$ and $^5D_1 \rightarrow {}^7F_0$. The information can be used as a firm basis for the exploration of doped and complex oxide luminescent materials containing Eu^{3+} ions.

■ ASSOCIATED CONTENT

Supporting Information

Structural cif file, Raman spectrum decomposition, and Raman spectra recorded with excitation at 457.9 and 514.5 nm. This material is available free of charge via the Internet at http://pubs.acs.org.

■ AUTHOR INFORMATION

Notes

The authors declare no competing financial interest.

■ ACKNOWLEDGMENTS

This study is partly supported by the Ministry of Education and Science of the Russian Federation.

■ REFERENCES

(1) Borchardt, H. J.; Bierstedt, P. E. Ferroelectric Rare-Earth Molybdates. *J. Appl. Phys.* **1967**, *38*, 2057−2060.

(2) Tripathi, A. K.; Lal, H. B. Electrical Transport in Rare-Earth Molybdates: $Gd_3(MoO_4)_3$ and $Tb_2(MoO_4)_3$. *J. Phys. Soc. Jpn.* **1980**, *49*, 1896−1901.

(3) Efremov, V. A. Characteristic Features of the Crystal Chemistry of Lanthanide Molybdates and Tungstates. *Russ. Chem. Rev.* **1990**, *59*, 627−642.

(4) Dmitriev, V.; Sinitsyn, V.; Dilanian, R.; Machon, D.; Kuznetsov, A.; Ponyatovsky, E.; Lucazeau, G.; Weber, H. P. In Situ Pressure-Induced Solid-State Amorphization in $Sm_2(MoO_4)_3$, $Eu_2(MoO_4)_3$ and $Gd_2(MoO_4)_3$ Crystals: Chemical Decomposition Scenario. *J. Phys. Chem. Solids* **2003**, *64*, 307−312.

(5) Bazarov, B. G.; Klevtsova, R. F.; Chimitova, O. D.; Glinskaya, I. A.; Fedorov, K. N.; Tushinova, Y. L.; Bazarova, Z. G. Phase Formation in the Rb_2MoO_4-$Er_2(MoO_4)_3$-$Hf(MoO_4)_2$ System and the Crystal Structure of New Triple Molybdate $Rb_5ErHf(MoO_4)_6$. *Russ. J. Inorg. Chem.* **2006**, *51*, 800−804.

(6) Xia, Z. G.; Chen, D. M. Synthesis and Luminescence Properties of $BaMoO_4:Sm^{3+}$ Phosphors. *J. Am. Ceram. Soc.* **2010**, *93*, 1397−1401.

(7) Mączka, M.; Majchrowski, A.; Kityk, I. V. Vibrational Properties of the Nonlinear Crystal β-$BaTeMo_2O_9$. *Vib. Spectrosc.* **2013**, *64*, 158−163.

(8) Chimitova, O. D.; Atuchin, V. V.; Bazarov, B. G.; Molokeev, M. S.; Bazarova, Z. G. The Formation and Structural Parameters of New Double Molybdates $RbLn(MoO_4)_2$ (Ln = Pr, Nd, Sm, Eu). *Proc. SPIE* **2013**, *8771*, 87711A.

(9) Hanuza, J.; Macalik, L.; Hermanowicz, K. Vibrational Properties of $KLn(MoO_4)_2$ Crystals for Light Rare Earth Ions from Lanthanum to Terbium. *J. Mol. Struct.* **1994**, *319*, 17−30.

(10) Macalik, L. Comparison of the Spectroscopic and Crystallographic Data of Tm^{3+} in the Different Hosts: $KLn(MoO_4)_2$ Where Ln = Y, La, Lu and M = Mo, W. *J. Alloys Compd.* **2002**, *341*, 226−232.

(11) Kato, A.; Oishi, S.; Shishido, T.; Yamazaki, M.; Iida, S. Evaluation of Stoichiometric Rare-Earth Molybdate and Tungstate Compounds as Laser Materials. *J. Phys. Chem. Solids* **2005**, *66*, 2079−2081.

(12) Chimitova, O. D.; Bazarov, B. G.; Klevtsova, R. F.; Anshits, A. G.; Fedorov, K. N.; Dubentsov, A. V.; Vereshchagina, T. A.; Tushinova, Y. L.; Glinskaya, L. A.; Bazarova, Z. G.; et al. Crystal Structure of Triple Molybdate in the Rb_2MoO_4-$Nd_2(MoO_4)_3$-$Zr(MoO_4)_2$ System. *J. Struct. Chem.* **2010**, *51*, 173−176.

(13) Tang, J. F.; Chen, Y. J.; Lin, Y. F.; Gong, X. H.; Huang, J. H.; Luo, Z. D.; Huang, Y. D. Polarized Spectral Properties and Laser Demonstration of Tm^{3+}-doped $LiGd(MoO_4)_2$ Crystal. *J. Opt. Soc. Am. B* **2010**, *27*, 1769−1777.

(14) Atuchin, V. V.; Grossman, V. G.; Adichtchev, S. V.; Surovtsev, N. V.; Gavrilova, T. A.; Bazarov, B. G. Structural and Vibrational Properties of Microcrystalline $TlM(MoO_4)_2$ (M = Nd, Pr) Molybdates. *Opt. Mater.* **2012**, *34*, 812−816.

(15) Lim, C. S. Synthesis and Characterization of Upconversion Photoluminescence Er^{3+}, Yb^{3+} Co-doped $SrMoO_4$ Particles via Microwave-Assisted Metathetic Route. *Asian J. Chem.* **2012**, *24*, 5662−5664.

(16) Atuchin, V. V.; Chimitova, O. D.; Adichtchev, S. V.; Bazarov, B. G.; Gavrilova, T. A.; Molokeev, M. S.; Surovtsev, N. V.; Bazarova, Zh. G. Synthesis, Structural and Vibrational Properties of Microcrystalline β-$RbSm(MoO_4)_2$. *Mater. Lett.* **2013**, *106*, 26−29.

(17) Lin, C. C.; Liu, R.-S. Advances in Phosphors for Light-Emitting Diodes. *J. Phys. Chem. Lett.* **2011**, *2*, 1268−1277.

(18) Luo, Y.; Xia, Z. G. Structural and Luminescence Properties of Sr_2VO_4Cl and $Sr_5(VO_4)_3Cl$: Self-Activated Luminescence and Unusual Eu^{3+} Emission. *RSC Adv.* **2013**, *3*, 22206−22212.

(19) Ko, Y. H.; Lee, S. H.; Yu, J. S. Luminescence Properties of Europium Ions-Doped Yttrium Silicate ($Y_2SiO_5:Eu^{3+}$) Nanocrystalline Phosphors: Effect of Eu^{3+} Ion Concentration and Thermal Annealing. *J. Nanosci. Nanotechnol.* **2013**, *13*, 3230−3235.

(20) Xia, Z. G.; Zhang, Y. Y.; Molokeev, M. S.; Atuchin, V. V. Structural and Luminescence Properties of Yellow-Emitting $NaSc$-$Si_2O_6:Eu^{2+}$ Phosphors: Eu^{2+} Site Preference Analysis and Generation of Red Emission by Codoping Mn^{2+} for White-Light-Emitting Diode Applications. *J. Phys. Chem. C* **2013**, *117*, 20847−20854.

(21) Chen, X.; Xia, Z. G. Luminescence Properties of $Li_2Ca_2ScV_3O_{12}$ and $Li_2Ca_2ScV_3O_{12}:Eu^{3+}$ Synthesized by Solid State Reaction Method. *Opt. Mater.* **2013**, *35*, 2736−2739.

(22) Tanner, P. A. Some Misconceptions Concerning the Electronic Spectra of Tri-positive Europium and Cerium. *Chem. Soc. Rev.* **2013**, *42*, 5090−5101.

(23) Xia, Z. G.; Zhang, Y. Y.; Molokeev, M. S.; Atuchin, V. V. Linear Structural Evolution Induced Tunable Photoluminescence in Clinopyroxene Solid-Solution Phosphors. *Sci. Rep.* **2013**, *3*, 3310.

(24) Li, G. G.; Lin, C. C.; Chen, W.-T.; Molokeev, M. S.; Atuchin, V. V.; Chiang, C.-Y.; Zhou, W. Z.; Wang, C.-W.; Li, W.-H.; Sheu, H.-S.; et al. Photoluminescence Tuning via Cation Substitution in Oxonitridosilicate Phosphors: DFT Calculations, Different Site Occupations, and Luminescence Mechanisms. *Chem. Mater.* **2014**, *26*, 2991−3001.

(25) Boulahya, K.; Parras, M.; Gonzalez-Calbet, J. M. Synthesis, Structural and Magnetic Characterization of a New Scheelite Related Compound: $Eu_2Mo_3O_{12}$. *Eur. J. Inorg. Chem.* **2005**, *2005*, 967−970.

(26) Nassau, K.; Levinstein, H. J.; Loiacono, G. M. A Comprehensive Study of Trivalent Tungstates and Molybdates of the Type $L_2(MoO_4)_3$. *J. Phys. Chem. Solids* **1965**, *26*, 1805−1816.

(27) Saleem, S. S.; Srinivasan, T. K. Laser Raman and Far-infrared Spectra of $Gd_2(MoO_4)_3$, $Tb_2(MoO_4)_3$, $GdTb(MoO_4)_3$, $GdDy(MoO_4)_3$, $Tb_{1.8}Eu_{0.2}(MoO_4)_3$, and $Gd_{0.2}Dy_{0.9}Tb_{0.9}(MoO_4)_3$ Single Crystals in the External Mode Region. *Spectrochim. Acta, Part A* **1985**, *41*, 1419−1425.

(28) Buijs, M.; Blasse, G. Nonresonant Energy Transfer in a System with Two Different Rare-Earth Sites: β'-$Gd_2(MoO_4)_3:Eu^{3+}$ and β'-$Eu_2(MoO_4)_3$. *Phys. Rev. B: Condens. Matter Mater. Phys.* **1986**, *34*, 8815−8821.

(29) Xue, D.; Betzler, K.; Hesse, H.; Lammers, D. Linear and Nonlinear Optical Susceptibilies of Orthorhombic Rare Earth Molybdates $RE_2(MoO_4)_3$. *J. Phys. Chem. Solids* **2002**, *63*, 359−361.

(30) Brixner, L. H. On the Structural and Physical Properties of the $Ln_2(MoO_4)_3$ and Ln_2MoO_6 Type Rare Earth Molybdates. *Rev. Chim. Miner.* **1973**, *10*, 47−61.

(31) Ozawa, T. C.; Kang, S. J. *Balls&Sticks*: Easy-to-use Structure Visualization and Animation Program. *J. Appl. Crystallogr.* **2004**, *37*, 679.

(32) Templeton, D. H.; Zalkin, A. Crystal Structure of Europium Tungstate. *Acta Crystallogr.* **1963**, *16*, 762−766.

(33) Boulahya, K.; Parras, M.; González-Calbet, J. M. A Structural Study of the Solid Solution $Eu_2(Mo_{1-x}W_x)_3O_{12}$. *Z. Anorg. Allg. Chem.* **2005**, *631*, 1988−1990.
(34) Brixner, L. H.; Bierstedt, P. E.; Sleight, A. W.; Licis, M. S. Precision Parameters of Some $Ln_2(MoO_4)_3$-type Rare Earth Molybdates. *Mater. Res. Bull.* **1971**, *6*, 545−554.
(35) Machon, D.; Dmitriev, V. P.; Sinitsyn, V. V.; Lucaseau, G. $Eu_2(MoO_4)_3$ Single Crystal at High Pressure: Structural Phase Transitions and Amorphization Probed by Fluorescence Spectroscopy. *Phys. Rev. B: Condens. Matter Mater. Phys.* **2004**, *70*, 094117.
(36) Shmurak, S. Z.; Kiselev, A. P.; Sinitsyn, V. V.; Shmit'ko, I. M.; Aronin, A. S.; Red'kin, B. S.; Ponyatovskii, E. G. Optical Spectroscopy of Europium Molybdate in the Crystalline and Amorphous States. *Phys. Solid State* **2006**, *48*, 51−57.
(37) Le Bacq, O.; Machon, D.; Testemale, D.; Pasturel, A. Pressure-Induced Amorphization Mechanism in $Eu_2(MoO_4)_3$. *Phys. Rev. B: Condens. Matter Mater. Phys.* **2011**, *83*, 214101.
(38) Lal, H. B.; Singh, M. On the Magnetic Susceptibility of Samarium and Europium Molybdates and Tungstates. *J. Magn. Magn. Mater.* **1981**, *25*, 56−60.
(39) *TOPAS*, V4; general profile and structure analysis software for powder diffraction data, user's manual. Bruker AXS: Karlsruhe, Germany, 2008.
(40) Malakhovskii, A. V.; Kutsak, T. V.; Sukharev, A. L.; Aleksandrovsky, A. S.; Krylov, A. S.; Gudim, I. A.; Molokeev, M. S. Spectroscopic Properties of $ErAl_3(BO_3)_4$ Single Crystals. *Chem. Phys.* **2014**, *428*, 137−143.
(41) Krylov, A. S.; Goryainov, S. V.; Laptash, N. M.; Vtyurin, A. N.; Melnikova, S. V.; Krylova, S. N. Influence of the Molecular Groups Ordering on Structural Phase Transitions in $(NH_4)_2WO_2F_4$. *Cryst. Growth Des.* **2014**, *14*, 374−380.
(42) Jansson, P. A. *Deconvolution: With Applications in Spectroscopy*; Academic Press: New York, 1984.
(43) Bazarov, B. G.; Chimitova, O. D.; Klevtsova, R. F.; Tushinova, Yu. L.; Glinskaya, L. A.; Bazarova, Z. G. Crystal Structure of a New Ternary Molybdate in the Rb_2MoO_4-$Eu_2(MoO_4)_3$-$Hf(MoO_4)_2$ System. *J. Struct. Chem.* **2008**, *49*, 53−57.
(44) Yakovlev, V. G.; Mikhailin, V. V.; Romanenko, A. Yu.; Basovich, O. M.; Khaikina, E. G. Spectral-Luminescent Properties of $LiRbLa_{2-x}Eu_x(MoO_4)_4$ Solid Solutions. *Moscow Univ. Phys. Bull. (Engl. Transl.)* **2010**, *65*, 392−396.
(45) Troitskaia, I. B.; Gavrilova, T. A.; Gromilov, S. A.; Sheglov, D. V.; Atuchin, V. V.; Vemuri, R. S.; Ramana, C. V. Growth and Structural Properties of α-MoO_3(010) Microplates with Atomically Flat Surface. *Mater. Sci. Eng., B* **2010**, *174*, 159−163.
(46) Atuchin, V. V.; Chimitova, O. D.; Gavrilova, T. A.; Molokeev, M. S.; Kim, S.-J.; Surovtsev, N. V.; Bazarov, B. G. Synthesis, Structural and Vibrational Properties of Microcrystalline $RbNd(MoO_4)_2$. *J. Cryst. Growth* **2011**, *318*, 683−686.
(47) Atuchin, V. V.; Gavrilova, T. A.; Grigorieva, T. I.; Kuratieva, N. V.; Okotrub, K. A.; Pervukhina, N. V.; Surovtsev, N. V. Sublimation Growth and Vibrational Microspectrometry of α-MoO_3 Single Crystals. *J. Cryst. Growth* **2011**, *318*, 987−990.
(48) Hayashi, S.; Sugano, H.; Arai, H.; Yamamoto, K. Phase Transitions in Gas-Evaporated WO_3 Microcrystals: A Raman Study. *J. Phys. Soc. Jpn.* **1992**, *61*, 916−923.
(49) Zaytsev, V. B.; Zhukova, A. A.; Rumyantseva, M. N.; Dobrovolsky, A. A.; Calvo, L.; Gaskov, A. M. Antimony Doped Whiskers of SnO_2 Grown from Vapor Phase. *J. Cryst. Growth* **2010**, *312*, 386−390.
(50) Löffler, S.; Auer, E.; Weil, M.; Lugstein, A.; Bertagnolli, E. Impact of Growth Temperature on the Crystal Habits, Forms and Structures of VO_2 Nanocrystals. *Appl. Phys. A: Mater. Sci. Process.* **2011**, *102*, 201−204.
(51) Li, C.; Huang, L.; Snigdha, G. P.; Yu, Y. F.; Cao, L. Y. Role of Boundary Layer Diffusion in Vapor Deposition Growth of Chalcogenide Nanosheets: The Case of GeS. *ACS Nano* **2012**, *6*, 8868−8877.
(52) Atuchin, V. V.; Gavrilova, T. A.; Kokh, K. A.; Kuratieva, N. V.; Pervukhina, N. V.; Surovtsev, N. V. Structural and Vibrational Properties of PVT Grown Bi_2Te_3 Microcrystals. *Solid State Commun.* **2012**, *152*, 1119−1122.
(53) Jeitschko, W. A comprehensive X-ray Study of the Ferroelectric-Ferroelastic and Paraelectric-Paraelastic Phases of $Gd_2(MoO_4)_3$. *Acta Crystallogr., Sect. B: Struct. Sci.* **1972**, *29*, 60−76.
(54) Atuchin, V. V.; Aleksandrovsky, A. S.; Chimitova, O. D.; Krylov, A. S.; Molokeev, M. S.; Bazarov, B. G.; Bazarova, J. G.; Xia, Z. G. Synthesis and Spectroscopic Properties of Multiferroic β'-$Tb_2(MoO_4)_3$. *Opt. Mater.* **2014**, *36*, 1631−1635.
(55) Smirnov, M. B.; Kazimirov, V. Yu. *LADY: Software for Lattice Dynamics Simulations*. JINR Communications, E 14-2001-159, 2001.
(56) Smirnov, M.; Baddour-Hadjean, R. Li Intercalation in TiO_2 Anatase: Raman Spectroscopy and Lattice Dynamic Studies. *J. Chem. Phys.* **2004**, *121*, 2348−2355.
(57) Vtyurin, A. N.; Krylov, A. S.; Krylova, S. N.; Goryainov, S. V.; Voronov, V. N.; Oreshonkov, A. S. Hydrostatic Pressure-Induced Phase Transitions in Rb_2KInF_6 and Rb_2KScF_6 Crystals: Raman Spectra and Lattice Dynamics Simulations. *Ferroelectrics* **2012**, *440*, 100−104.
(58) Krylov, A. S.; Vtyurin, A. N.; Oreshonkov, A. S.; Voronov, V. N.; Krylova, S. N. Structural Transformations in Single Crystal Rb_2NaYF_6: Raman Scattering Study. *J. Raman Spectrosc.* **2013**, *44*, 763−769.
(59) Gerasimova, Y. V.; Oreshonkov, A. S.; Vtyurin, A. N.; Ivanenko, A. A.; Isaenko, L. I.; Ershov, A. A.; Pogoreltsev, E. I. Infrared Absorption Investigation of the Role of Octahedral Groups upon the Phase Transition in the $Rb_2KMoO_3F_3$ Crystal. *Phys. Solid State* **2013**, *55*, 2331−2334.
(60) Xia, Z. G.; Molokeev, M. S.; Oreshonkov, A. S.; Atuchin, V. V.; Liu, R.-S.; Dong, C. Crystal and Local Structure Refinement in $Ca_2Al_3O_6F$ Explored by X-ray Diffraction and Raman Spectroscopy. *Phys. Chem. Chem. Phys.* **2014**, *16*, 5952−5957.
(61) Nakomoto, K. *Infrared and Raman Spectra of Inorganic and Coordination Compounds*, 6th ed.; Wiley: New York, 2009.
(62) Raju, G. S. R.; Pavitra, E.; Nagaraju, G. P.; Kandimalla, R.; El-Rayes, B. F.; Yu, J. S. PEGylated α-$Gd_2(MoO_4)_3$ Mesoporous Flowers: Synthesis, Characterization, and Biological Application. *Cryst. Growth Des.* **2013**, *13*, 4051−4058.
(63) Cho, Y.-S.; Kim, D.; Lee, Y.-J.; Yang, H.; Huh, Y.-D. Preparation and Photoluminescence Properties of Red-Emitting $Gd_2(MoO_4)_3$:Eu Phosphors for a Three-Band White LED. *Bull. Korean Chem. Soc.* **2010**, *31*, 2992−2994.
(64) Buijs, M.; Blasse, G.; Brixner, L. H. Nonresonant Energy Transfer in a System with Two Different Rare-Earth Sites: β'-$Gd_2(MoO_4)_3$:Eu^{3+} and β'-$Eu_2(MoO_4)_3$. *Phys. Rev. B: Condens. Matter Mater. Phys.* **1986**, *34*, 8815−8821.